Nonlinear optical contrast enhancement for optical coherence tomography

Claudio Vinegoni, Jeremy S. Bredfeldt, and Daniel L. Marks

Beckman Institute for Advanced Science and Technology, University of Illinois at Urbana-Champaign

Stephen A. Boppart

Department of Electrical and Computer Engineering
Beckman Institute for Advanced Science and Technology, Department of Bioengineering
College of Medicine
University of Illinois at Urbana-Champaign, 405 N. Mathews Ave., Urbana, IL 61801
boppart@uiuc.edu

http://nb.beckman.uiuc.edu/biophotonics/

Abstract: We present a new interferometric technique for measuring Coherent Anti-Stokes Raman Scattering (CARS) and Second Harmonic Generation (SHG) signals. Heterodyne detection is employed to increase the sensitivity in both CARS and SHG signal detection, which can also be extended to different coherent processes. The exploitation of the mentioned optical nonlinearities for molecular contrast enhancement in Optical Coherence Tomography (OCT) is presented.

OCIS codes: (111.4500) Optical coherence tomography; (300.6230) Spectroscopy, coherent anti-Stokes Raman scattering; (190.4410) Nonlinear optics, parametric processes; (120.3180) Interferometry; (040.2840) Heterodyne; (190.4160) Multiharmonic generation.

References and links

1. D. Huang, E. A. Swanson, C. P. Lin, J. S. Schuman, W. G. Stinson, W. Chang, M. R. Hee, T. Flotte, K. Gregory, C. A. Puliafto, and J. G. Fujimoto, "Optical coherence tomography," Science **254**, 1178–1181 (1991).
2. S. A. Boppart, B. E. Bouma, C. Pitris, J. F. Southern, M. E. Brezinski, and J. G. Fujimoto, "*In vivo* cellular optical coherence tomography imaging," Nat. Med. **4**, 861–5 (1998).
3. Y. Wang, Y. Zhao, Z. Chen, R. S. Windeler, and J. Nelson, "Ultrahigh-resolution optical coherence tomography by broadband continuum generation from a photonic crystal fiber," Opt. Lett. **28**, 182–184 (2003).
4. J. G. Fujimoto, "Optical coherence tomography for ultrahigh resolution *in vivo* imaging," Nat. Biotechnol. **21**, 1361–1367 (2003).
5. T. M. Lee, A. L. Oldenburg, S. Sitafalwalla, D. L. Marks, W. Luo, F. J.-J. Toublan, K. S. Suslick, and S. A. Boppart, "Engineered microsphere contrast agents for optical coherence tomography," Opt. Lett. **28**, 1546–1548 (2003).
6. U. Morgner, W. Drexler, F. Kartner, X. Li, C. Pitris, E. Ippen, and J. Fujimoto, "Spectroscopic optical coherence tomography," Opt. Lett. **25**, 111–13 (2000).
7. K. Divakar Rao, M. A. Choma, S. Yazdanfar, A. M. Rollins, and J. A. Izatt, "Molecular contrast in optical coherence tomography by use of a pump-probe technique," Opt. Lett. **28**, 340–2 (2003).
8. J. K. Barton, J. B. Hoying, and C. J. Sullivan, "Use of microbubbles as an optical coherence tomography contrast agent," Acad. Radiol. **9**, S52–5 (2002).
9. R. K. Chang, J. Ducuing, and N. Bloembergen, "Relative phase measurement between fundamental and second-harmonic light," Phys. Rev. Lett. **15**, 6–9 (1965).
10. R. Stolle, G. Marowsky, E. Schwarzberg, and G. Berkovic "Phase measurements in nonlinear optics," Appl. Phys. B **63**, 491–8 (1996).
11. G. Marowsky, and G. Luepke "CARS-background suppression by phase-controlled nonlinear interferometry," Appl. Phys. B **51**, 49–51 (1990).

#3545 - $15.00 US Received 17 December 2003; revised 15 January 2004; accepted 15 January 2004

12. J.W. Hahn, and E.S. Lee "Measurement of nonresonant third-order susceptibilities of various gases by the nonlinear interferometric technique," JOSA B **12**, 1021–27 (1995).
13. A. Zumbusch, G. Holtorn, and X. Sunney Xie, "Three-dimensional vibrational imaging by coherent anti-Stokes Raman scattering," Phys. Rev. Lett. **82**, 4142–5 (1999).
14. W. Dermtroeder, *Laser Spectroscopy* (Springer, 1998).
15. J.-X. Cheng, A. Volkmer, and X. Xie, "Theoretical and experimental characterization of coherent anti-Stokes Raman scattering microscopy," J. Opt. Soc. Am. B **19**, 1363–75 (2002).
16. M. Duncan, J. Reintjes, and T. Manuccia, "Scanning coherent anti-Stokes Raman microscope," Opt. Lett. **7**, 350–2 (1982).
17. G. W. Wurpel, J. M. Schins, and M. Muller, "Chemical specificity in three-dimensional imaging with multiplex coherent anti-Stokes Raman scattering microscopy," Opt. Lett. **27**, 1093–1095 (2002).
18. M. Hashimoto, T. Araki, and S. Kawata, "Molecular vibration imaging in the fingerprint region by use of coherent anti-Stokes Raman scattering microscopy with a collinear configuration," Opt. Lett. **25**, 1768–1770 (2000).
19. J.-X. Cheng, Y. Kevin Jia, G. Zheng, and X. Xie, "Laser–scanning coherent anti-Stokes Raman scattering microscopy and applications to cell biology," Biophys. Journal **83**, 502–9 (2002).
20. D. L. Marks and S. A. Boppart, "Nonlinear interferometric vibrational imaging: theory and simulations," In Press, Phys. Rev. Lett.; LANL E–print arXive http://www.arxiv.org/abs/physics/0311071 (2003).
21. D. L. Marks, J. Bredfeldt, S. Hambir, D. Dlott, B. Kitchell, M. Gruebele, and S. A. Boppart, "Molecular species sensitive optical coherence tomography using coherent anti-Stokes Raman scattering spectroscopy," in *Coherence domain optical methods and OCT in biomedicine VII*, V.V. Tuchin, J.A. Izatt, and J.G. Fujimoto, eds., Proc. SPIE **4956,** 9–13 (2003).
22. J. Bredfeldt, D. L. Marks, C. Vinegoni, S. Hambir, and S. A. Boppart, "Coherent anti-Stokes Raman scattering heterodyne interferometry," Submitted; LANL E–print arXive http://www.arxiv.org/abs/physics/0311057 (2003).
23. P. J. Campagnola and L. M. Loew, "Second-harmonic imaging microscopy for visualizing biomolecular arrays in cells, tissues and organisms," Nat. Biotechnol. **21**, 1356–1360 (2003).
24. P. Stoller, P. M. Celliers, K. M. Reiser, and A. M. Rubenchik, "Quantitative second-harmonic generation microscopy in collagen," Appl. Optics **42**, 5209–5219 (2003).
25. I. Freund and M. Deutsch, "Connective tissue polarity. Optical second-harmonic microscopy, crossed-beam summation, and small-angle scattering in Rat-tail tendon," Biophys. J. **50**, 693–712 (1986).
26. K. Eisenthal, "Liquid Interfaces Probed by Second-Harmonic and Sum-Frequency Spectroscopy," Chem. Rev. **96**, 1343–60 (1996).
27. R. Brown, A. Millard, and P. J. Campagnola, "Macromolecular structure of cellulose studied by second-harmonic generation imaging microscopy. " Opt. Lett. **28**, 2207–2209 (2003).
28. J. Squier, M. Muller, G. Brakenhoff, and K. Wilson, "Third harmonic generation microscopy," Opt. Express **3**, 315 –24 (1998), http://www.opticsexpress.org/abstract.cfm?URI=OPEX-3-9-315

1. Introduction

Optical coherence tomography (OCT) is an emerging biomedical imaging technology that has been applied to a wide range of biological, medical, and materials investigations. OCT was first developed in the early 1990s for noninvasive imaging of biological tissue [1] and is capable of imaging tissue microstructures at near histological resolutions [2]. Axial resolution of 10 μm is common for standard OCT, whereas for ultrahigh resolution OCT, an axial resolution in the 1 μm range has been recently achieved using broadband-continuum generation from a photonic crystal fiber [3].

The advantages of OCT in biomedical imaging, compared to other imaging techniques, are quite numerous [4]. In particular, OCT can provide imaging resolutions that approach those of conventional histopathology and can be performed *in situ* [4]. Despite its advantages, a serious drawback to OCT is that the linear scattering properties of pathological tissue probed by OCT are often morphologically and/or optically similar to the scattering properties of normal tissue. For example, although morphological differences between normal and neoplastic tissues may be obvious at later stages of tumor development, it is frequently difficult to optically detect early-stage tumors [5].

Novel contrast enhancing mechanisms for OCT are needed to help differentiate tissue types that are frequently morphologically or optically similar when using current OCT methods. Examples of methods that have been recently developed include: spectroscopic OCT (SOCT) [6], pump and probe techniques [7], and the use of engineered microspheres [5] or microbub-

#3545 - $15.00 US Received 17 December 2003; revised 15 January 2004; accepted 15 January 2004

bles [8]. Spectroscopic OCT measures the spectral absorption and/or scattering from tissues by measuring the spectral differences between the source and the backscattered interference signal to provide information about the properties of the sample. However, this technique is limited to the identification of features that have absorption scattering within the bandwidth of the optical source. Pump and probe contrast enhancement for OCT imaging relies on transient absorptions in the sample under investigation that are induced by an external pump beam. Unfortunately, it is necessary in most cases to introduce different contrast agents depending on the excitation source and on the transient spectra of the molecules under investigation [7]. An alternative way to obtain contrast enhancement in OCT includes the use of exogenous contrast agents such as engineered microspheres. These microspheres change the optical scattering or absorption characteristics in selected regions and can be targeted to cell receptors, providing molecular specific contrast [5]. Most of the methods (if not all) that are currently used to enhance contrast imaging in OCT require the presence of a contrast agent, which can modify the biology under investigation. Therefore there is a need for new techniques that could help eliminate this limitation.

In this paper, we propose and present new methods to achieve enhanced OCT contrast by exploiting optical nonlinearities. The nonlinear processes, in particular, are Coherent Anti-Stokes Raman Scattering (CARS) and Second Harmonic Generation (SHG), but the general idea could be easily extended to other nonlinear processes such as Third Harmonic Generation (THG), Coherent Stokes Raman Spectroscopy (CSRS), and stimulated emission in active materials (i.e. InGaAs, GaAs based materials, etc.). The principle of operation is based on nonlinear interferometry, a technique first proposed by Chang *et al.* in 1965 [9]. Second harmonic generation signals were interfered to determine the phase of the χ^2 of the medium. The same technique was later refined in other works for both SHG [10] and CARS [11, 12]. We propose a method which exploits nonlinear interferometry using broadband illumination for imaging purposes, and in particular, as a molecularly-specific contrast enhancing method for OCT.

2. CARS contrast enhancement

2.1. Theory

It is well known that the nonlinear polarization for a material can be expressed as a function of the incident electric field vector $\bar{E}$:

$$\bar{P} = \varepsilon_0 \left(\chi^{(1)} \cdot \bar{E} + \chi^{(2)} : \bar{E}\bar{E} + \chi^{(3)} \vdots \bar{E}\bar{E}\bar{E} + \ldots \right) \tag{1}$$

with $\bar{P}$ as the induced polarization, $\chi^{(n)}$ as the n-th order nonlinear susceptibility, and ε_0 as the vacuum permittivity. This implies that for high intensities (i.e. in a nonlinear regime) the induced polarization is no longer directly proportional to the incoming electric field vector $\bar{E}$. Usually the first term $\chi^{(1)}$ represents the main contribution to $\bar{P}$ and describes linear effects as absorption or reflection. The second term is responsible for nonlinear effects like SHG and sum-frequency generation which we will consider in Sect. 3. The third term $\chi^{(3)}$ is responsible for phenomena involving four photons, like CARS, four wave mixing (FWM), third harmonic generation (THG), and nonlinear refraction.

In this section we focus on CARS, a spectroscopic technique that has recently received increasing attention for its applications for vibrational imaging [13]. In CARS spectroscopy, the frequencies of two incident lasers, ω_p and ω_s (Pump and Stokes, respectively), are selected such that the difference in frequency ω_p-ω_s= ω_v is equal to the frequency of a Raman-active vibrational mode present in the molecule under study [14]. As evident from Eq.1, CARS is a nonlinear, four-wave mixing process. The CARS field therefore, is a result of the interaction

#3545 - $15.00 US Received 17 December 2003; revised 15 January 2004; accepted 15 January 2004

between four photons and is generated in the phase-matching direction at the anti-Stokes frequency $\omega_{AS} = 2\omega_p - \omega_s$, implying that the CARS signal intensity is linearly dependent on the Stokes field intensity and quadratically dependent on the pump field intensity. Note that CARS is a coherent process, with the phase of the anti-Stokes field related to the phase of the excitation field. Therefore, constructive interference of the anti-Stokes field causes the CARS signal to be significantly larger than the spontaneous Raman signal, given the same average excitation power [15]. All these characteristics have allowed CARS to be successfully employed to provide vibrational contrast in scanning microscopy [13, 15, 16, 17]. CARS microscopy generally involves scanning overlapped and tightly focused pump and Stokes beams through a sample while measuring the anti-Stokes signal amplitude point by point [18]. The first CARS microscope [16] used non-collinear visible-wavelength pump and Stokes beams to prove microscopic imaging of the spatial distribution of deuterated molecular bonds in a sample of onion skin.

Picosecond lasers were used by Hashimoto *et al.* [18] to improve the Raman spectral resolution and to further reduce the non-resonant background signal. Cheng *et al.* [15] theoretically evaluated the use of CARS in microscopy and recently used polarization, epi-directional, counter propagating, and forward CARS microscopy to study cell biology [19]. Multiplex CARS imaging has also been demonstrated to provide contrast based on one or more vibrational spectral features [17].

In each of these CARS microscopy techniques, the anti-Stokes photons are counted in order to estimate the density of the Raman scatterers in the focal volume of the microscope. Unfortunately, the spectral phase information is lost in this process. In this paper we present a new interferometric technique called Nonlinear Interferometric Vibrational Imaging (NIVI) [20] with the capability for heterodyne detection and the possibility to obtain a full reconstruction of the magnitude and phase of the sample Raman susceptibility [21, 22].

2.2. Experimental Setup

The laser system constructed to create the laser fields necessary to stimulate the CARS signal in the samples is shown in Fig. 1. A 6 W diode-pumped frequency-doubled Nd:YVO_4 laser

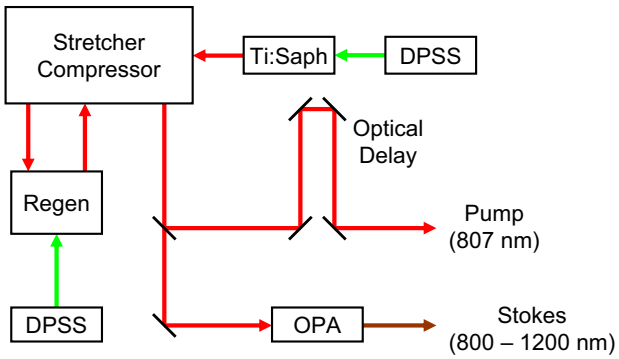

Fig. 1. Setup used to generate the Stokes and the Pump excitation fields. DPSS, diode-pumped solid-state laser; Regen, regenerative amplifier; OPA, optical parametric amplifier.

(Verdi, Coherent, Inc.) was used to pump a mode-locked Ti:sapphire oscillator (MTS, Kapteyn-

#3545 - $15.00 US Received 17 December 2003; revised 15 January 2004; accepted 15 January 2004

Murnane Labs, Inc.) operating at a center wavelength of 807 nm, with a bandwidth of 30 nm, a repetition rate of 82 MHz, and an average power of 300 mW. These pulses were sent to seed a regenerative chirped pulse amplifier (RegA 9000, Coherent, Inc.) that produced approximately 70 fs, 5 μJ pulses with a repetition rate of 250 kHz and an average power of 1.25 W. Around ten percent of this average power was used as the pump beam, and the remaining power was directed to an optical parametric amplifier (OPA 9400, Coherent, Inc.) which generated a 4 mW average power Stokes beam, tunable from 400-1200 nm [22].

Once the pump and the Stokes fields were generated, the two fields entered the interferometer shown in Fig. 2. An excitation field consisting of two overlapped pulses centered at the

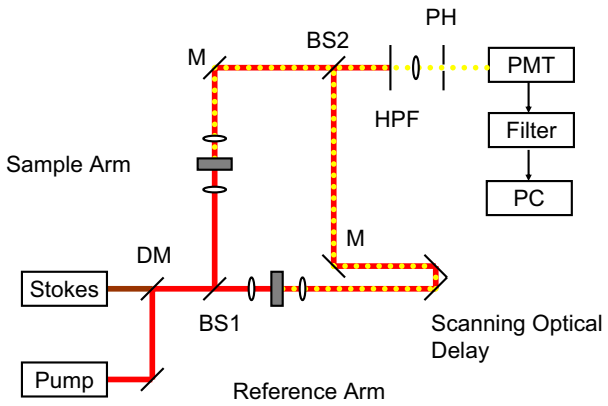

Fig. 2. Setup of the interferometric CARS measurement system. DM, dichroic mirror; BS, beamsplitter; M, mirror; HPF, high-pass-filter; PH, pin-hole; PMT photomultiplier tube; PC, personal computer.

pump and Stokes wavelengths was divided by a beamsplitter into two separate interferometer paths, which are referred to in Fig. 2 as the "sample arm" and "reference arm". A sample of a molecule was placed into each arm, and the split excitation fields were focused into these samples. When the Stokes pulses were tuned such that the difference in frequency between the pump and Stokes pulses was equal to a Raman active vibrational mode present in the molecule in both the sample arm and the reference arm, an anti-Stokes signal was generated in each arm of the interferometer. The anti-Stokes fields, being coherent with the incident fields, interfere at the beamsplitter BS2 when temporally and spatially overlapped.

The pump and the Stokes pulses, at 807 nm and 1072 nm respectively, were used to excite the Raman-active vibrational mode of benzene at 3063 cm^{-1}. The pulses were collinearly overlapped using a dichroic mirror and split with a 50:50 ultrafast beamsplitter (BS1) into the sample arm and the reference arm. In both arms, a 30 mm focal length, 12 mm diameter achromatic lenses were used to focus the pump and Stokes beams into the samples. The positions of the samples in each arm from the beamsplitter BS1 were equal. The anti-Stokes signals generated in each arm were collected in the collinear phase matching direction using a 30 mm focal length, 12 mm diameter singlet lenses. The two anti-Stokes signals were then overlapped in time by adjusting the relative delay, using a scanning opical delay line, and in space by adjusting their positions on a second beamsplitter (BS2). A high-pass filter at 742 nm was used to eliminate the remaining excitation light and the filtered anti-Stokes signals were spatially fil-

#3545 - $15.00 US Received 17 December 2003; revised 15 January 2004; accepted 15 January 2004

tered through a 50 μm diameter pin hole. The delay line in the reference arm was scanned by a computer-controlled single axis translation stage at a constant rate. The CARS signal intensity was measured with a photomultiplier tube (PMT)(HC 123, Hamamatsu, Corp.). The signal was finally filtered with a low-pass anti-aliasing filter and sampled with a PC based data acquisition system (NI DAQ, National Instruments).

2.3. Results and discussion

Initially the interferometer was calibrated with the pump signal only (λ = 807 nm). The acquired interferogram (Fig. 3) is shown for reference as a comparison with the following interferograms shown below. The interferogram was detected at the beamsplitter BS2 (Fig. 2) and was recorded as the pathlength of the reference arm was scanned. Having determined the

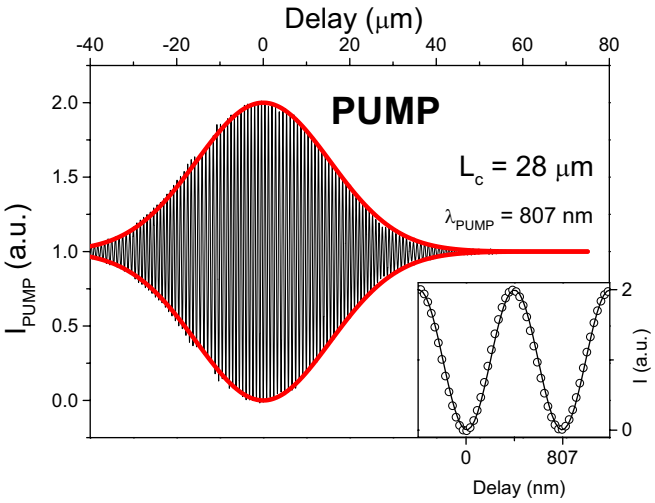

Fig. 3. Interferogram of the pump beam detected at the beamsplitter BS2 of the setup shown in Fig. 2. The envelope of the interferogram was fitted using the modulus of the degree of the coherence function. In the inset is shown a detail of the interference pattern and its fit by the real part of the degree of coherence function (open circles: experimental data; solid line: fit). L_c is the coherence length of the pulse. λ_{PUMP} is the wavelength of the Pump signal.

interferogram for the pump field, two quartz cuvettes filled with benzene were inserted in the two interferometer arms. To demonstrate that the signal collected from the cuvette was a CARS signal, Figs. 4(a) and 4(b) show the observed relationship between the CARS and the pump intensity (Stokes intensity fixed) and the CARS and the Stokes intensity (pump intensity fixed), respectively. In agreement with the theory, the slope of the fitted lines verify the linear relationship between the anti-Stokes and the Stokes intensities, and the quadratic relationship between the anti-Stokes and the pump intensities. This implies that our signal is a result of a four-wave mixing process. In addition, we observed that this process is CARS resonance because the anti-Stokes power is maximized when the Stokes wavelength is tuned to resonance with the Raman-active benzene vibrational mode.

Established that the filtered signals from both the cuvettes were CARS signals, the resulting signal at the beamsplitter BS2 of the setup shown in Fig. 2 was detected. The measured interferogram results from the interference between the two anti-Stokes signals and was recorded as the pathlength of the reference arm was scanned. The function used to fit the experimen-

#3545 - $15.00 US Received 17 December 2003; revised 15 January 2004; accepted 15 January 2004

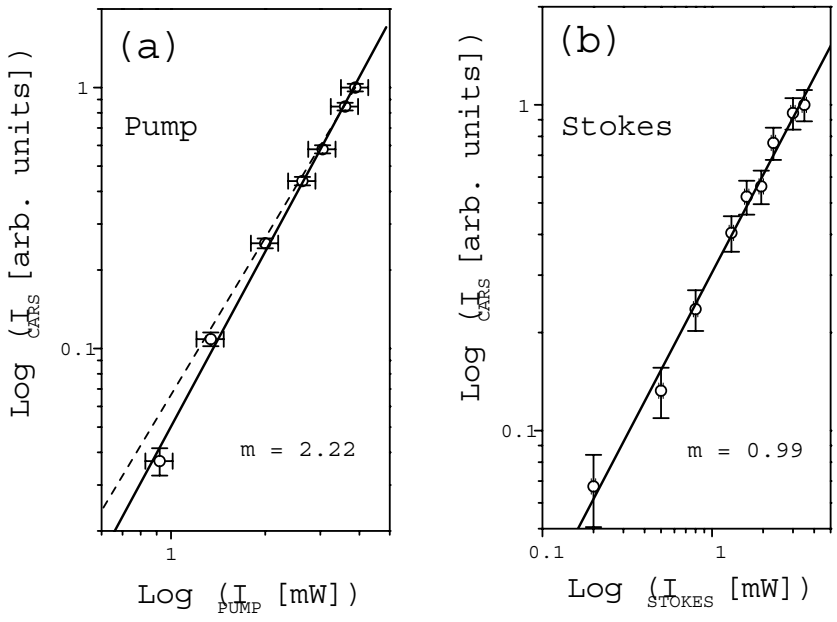

Fig. 4. Log-log plots of the intensity of the CARS signal as a function of (a) the intensity of the Pump field and (b) the intensity of the Stokes field (solid lines, curve fitting). The dotted line in (a) has a slope of 2. "m" is the angular coefficient of the solid lines [22].

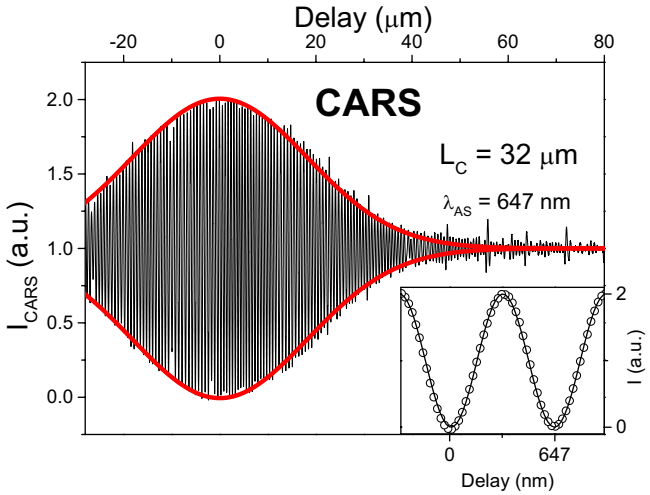

Fig. 5. CARS interferogram detected at the beamsplitter BS2 of the setup shown in Fig.2. The envelope of the interferogram was fitted using the modulus of the degree of the coherence function. In the inset is shown a detail of the interference pattern and its fit by the real part of the degree of coherence function (open circles: experimental data; solid line: fit). L_c is the coherence length of the pulse. λ_{AS} is the wavelength of the CARS signal.

#3545 - $15.00 US
Received 17 December 2003; revised 15 January 2004; accepted 15 January 2004

tal data is the degree of coherence function, that under the assumption of a Gaussian spectral distribution, is given by

$$\gamma(\tau) = \exp\left(-i\tau\omega_0 - i\frac{\delta\omega^2\tau^2}{4}\right) \tag{2}$$

where τ is the time, ω_0 is the center frequency and $\delta\omega$ is the bandwidth of the CARS pulse. The real part and the modulus of the coherence function, under the assumption of a Gaussian spectral distribution, were used to fit the experimental data (interferogram and envelope respectively) and are plotted in Fig. 5.

The resulting coherence length L_C, defined as the axial resolution of the interferometric CARS measurement technique, is equal to

$$\tau_c = \int_{-\infty}^{+\infty} |\gamma(\tau)|^2 d\tau \tag{3}$$

and was found to be equal to 32 μm.

The possibility to demodulate interferometrically the two anti-Stokes signals generated in separate samples demonstrates the potential of CARS as a promising technique for providing molecular contrast for OCT-like interferometric imaging systems. Interference indicates that similar Raman-active vibrational frequencies were present in both the reference and the sample arm. The "fingerprint" nature of Raman spectroscopy and the possibility to switch between different molecular species in the reference arm, could permit selective detection and imaging of different molecules in the sample. Moreover, the possibility to interfere a weak CARS signal with another strong CARS signal (produced in the reference arm), provides heterodyne sensitivity and an improved signal-to-noise ratio.

In our setup, low numerical aperture (NA) lenses were used to focus the beams into the cuvettes and to collect the CARS signals in the forward-directed, phase-matched direction. Recently it has been demonstrated that the use of high NA objectives, in order to achieve tight focusing, is particularly effective in CARS microscopy because it not only improves the imaging resolution but also allows for epi-detection of the CARS signal(i.e. collection of the CARS signal in backreflection). Epi-detection of CARS has been shown to be extremely efficient compared to forward collection, and useful for detecting the CARS signal from very small objects [15]. Epi-detection is advantageous for OCT because it provides both higher contrast and resolution. The collection of backscattered signal is particularly useful for imaging non-transparent tissues in more traditional OCT system configurations.

3. SHG contrast enhancement

3.1. Theory

Second Harmonic Generation, also known as frequency doubling, has recently emerged as a useful contrast mechanism for microscopic imaging of cell and tissue structures and functions [23]. As mentioned in Sec. 2.1 and in contrast to CARS, SHG is a $\chi^{(2)}$ process in which two photons at the fundamental frequency are converted into a single photon at exactly twice the frequency without having any absorption and/or re-emission from the sample [24].

The first biological SHG imaging experiment dates back to 1986 and involved the study of orientation of collagen fibers in a rat tail tendon [25]. Since then, SHG microscopy has been successfully applied in many different fields. In particular, SHG microscopy has been shown to be highly effective at selectively probing interfaces, while minimizing the signal coming from the bulk media [26]. The reason for this is that second-order processes are electric dipole forbidden in centrosymmetric media. This implies that bulk liquids and centrosymmetric crystalline solids do not generate second-harmonic signals. At the interfaces, the molecular and atomic

#3545 - $15.00 US Received 17 December 2003; revised 15 January 2004; accepted 15 January 2004

species experience different interactions and the inversion symmetry, which is present in the bulk, is broken [26]. Another advantage of SHG microscopy is the high resolution typically achieved in nonlinear microscopy, which has enabled applications for imaging structures in live tissues consisting of endogenous proteins such as collagen. Finally, it is important to note that the contrast enhancement in SHG microscopy is obtained without requiring the presence of any exogenous labels [27].

For all of these reasons, SHG microscopy is a good candidate for providing contrast enhancement for OCT. In the next section, we demonstrate that the interferometer presented in Section 2.1 can be simply modified and used for SHG heterodyne detection due to the fact that SHG, like CARS, is a process coherent with the excitation field.

3.2. Experimental Setup

The SHG interferometer is similar to the CARS interferometer and is shown in Fig. 6. Instead

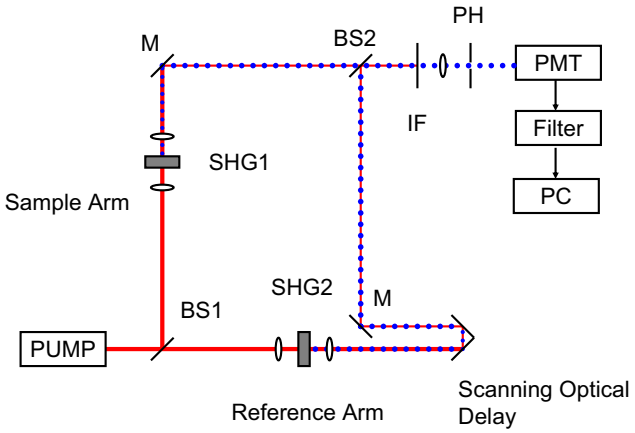

Fig. 6. Setup of the interferometric SHG measurement system. Two different SHG crystals (Type I) were inserted in the two arms of the interferometers. BS, beamsplitter; M, mirror; IF, interference filter; PH, pin-hole; PMT, photomultiplier tube; PC, personal computer.

of utilizing both Stokes and Pump lasers, only the Pump laser at 807 nm was present. In the reference arm, a reference SHG signal was created in a 100 μm nonlinear crystal (BBO, Type I). In the sample arm, a different nonlinear crystal (BBO, Type I) with a thickness of 1 mm was present. The signals generated in both crystals were overlapped as in the CARS configuration scheme.

Considering the general methodology presented here, when a SHG-generating crystal is placed in the reference arm, the SHG signal created in the sample under investigation and present in the sample arm can be heterodyne-detected, allowing for high sensitivity detection and OCT imaging.

3.3. Results and discussion

Figure 7 shows the measured interferogram resulting from the interference between the two SHG signals. This result indicates that two SHG signals generated in separate samples using the same pump laser can be demodulated interferometrically. In this case as well, the presence of interference clearly demonstrates the potential of SHG and resonance-enhanced SHG as a

#3545 - $15.00 US Received 17 December 2003; revised 15 January 2004; accepted 15 January 2004

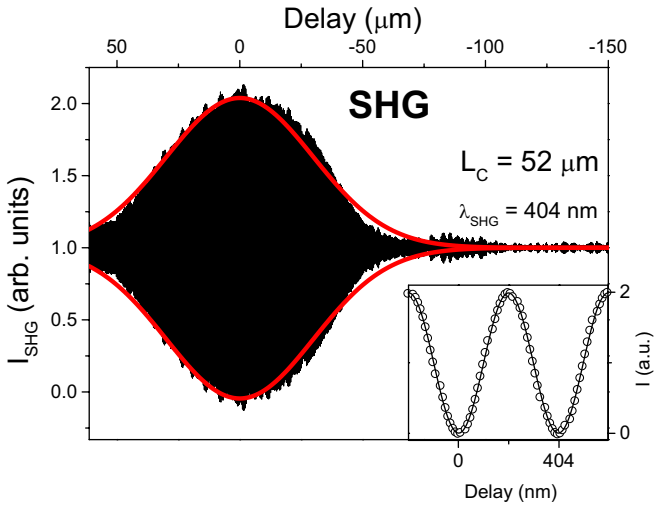

Fig. 7. SHG interferogram detected at the beamsplitter BS2 of the setup shown in Fig.6. The interferogram was recorded as the pathlength of the reference arm was scanned. The modulus of the degree of the coherence function was used to fit the envelope of the interferogram. The inset shows a detail of the interference pattern and its fit by the real part of the degree of coherence function (open circles: experimental data; solid line: fit). L_c is the coherence length of the pulse. λ_{SHG} is the wavelength of the SHG signal.

promising technique for providing molecular contrast for OCT-like interferometric imaging systems. The presence of a nonlinear crystal in the reference arm will allow one to interferometrically demodulate the SHG signal created in the sample under investigation.

4. Conclusion

In conclusion, we have described novel methods for contrast enhancement in OCT based on optical nonlinearities. The contrast mechanisms are based on resonant enhancement of the third order and second order nonlinear susceptibility of the molecules under investigation. The interference between two CARS signals generated in separate samples (or alternatively two SHG signals) was observed, allowing for heterodyne detection. The proposed interferometric scheme is very promising for the development of a new molecular imaging technique (NIVI) based on nonlinear low-coherence interferometry [20, 22] and for SHG-OCT.

In this work, we focused on forward CARS and SHG. Epi-detected CARS and SHG are coherent as well and are compatible with OCT coherence-ranging systems. CARS and SHG interferometry benefit from the advantages of interferometric detection while at the same time can enhance OCT images with molecular-specific contrast. These advantages could make CARS and SHG interferometry powerful tools for biological imaging with OCT. Moreover, the same configuration scheme could be exploited for Third Harmonic Generation (THG) microscopy [28], Coherent Stokes Raman Scattering (CSRS) microscopy, and other coherent scattering processes.

Acknowledgments

This research was supported in part by a research grant entitled ”A Nonlinear OCT System for Biomolecular Detection and Intervention” from NASA and the National Cancer Institute

(NAS2-02057, SAB). S.A. Boppart's email address is boppart@uiuc.edu.

#3545 - $15.00 US Received 17 December 2003; revised 15 January 2004; accepted 15 January 2004